Optical and microphysical properties of natural mineral dust and anthropogenic soil dust near dust source regions over Northwestern China

Xin Wang[1], Hui Wen[1], Jinsen Shi[1], Jianrong Bi[1], Zhongwei Huang[1], Beidou Zhang[1], Tian Zhou[1], Kaiqi Fu[1], Quanliang Chen[2], and Jinyuan Xin[3]

[1] Key Laboratory for Semi-Arid Climate Change of the Ministry of Education, College of Atmospheric Sciences, Lanzhou University, Lanzhou 730000, China

[2] Plateau Atmospheric and Environment Laboratory of Sichuan Province, College of Atmospheric Sciences, Chengdu University of Information Technology, Chengdu 610225, China

[3] State Key Laboratory of Atmospheric Boundary Layer Physics and Atmospheric Chemistry (LAPC), Institute of Atmospheric Physics, Chinese Academy of Sciences, Beijing 100029, China

Correspondence to: X. Wang (wxin@lzu.edu.cn)

Atmospheric
Chemistry
and Physics
Discussions

Open Access

EGU

Abstract.

From 3 April to 16 May 2014, a ground-based mobile laboratory was deployed to measure the optical and microphysical properties of tropospheric aerosols near dust source regions in Wuwei, Zhangye, and Dunhuang along the Hexi Corridor over

5   Northwestern China. This study is novel in that we not only captured natural mineral dust near the Taklimakan and Badain Jaran desert regions but also characterized the properties of anthropogenic soil dust produced by agricultural cultivations (e.g., land planning, ploughing, and disking), especially during floating dust episodes. In this dust campaign, the aerosol scattering (absorption) coefficient (σ_{sp} and σ_{ap}), single

10   scattering albedo (ω), scattering Ångström exponent (Å$_{sp}$), mass scattering efficiency (MSE), and aerosol size distribution were observed at 5-min intervals. The results indicate that large differences were found between the optical and microphysical properties of anthropogenic and natural dust because of floating dust episodes and dust storms. The values of σ_{sp}, σ_{ap} and ω of PM$_{2.5}$ measured at 550 nm range from ~37–

15   532 Mm^{-1}, ~2.2–55.3 Mm^{-1} and ~0.64–0.98, respectively, because of the presence of anthropogenic soil dust during floating dust episodes, and the corresponding values under background conditions are ~21–163 Mm^{-1}, ~1.3–34.8 Mm^{-1}, and ~0.70–0.98, respectively. We note that the higher values of σ_{sp} and ω and lower values of Å$_{sp}$ indicate that the aerosol particles observed during a strong dust storm in Zhangye were

20   dominated by coarse mode particles originating from desert regions. However, the highest values of MSE reveal that the anthropogenic soil dust produced by agricultural cultivations can scatter more solar radiation than coarse mode particles.

Atmospheric
Chemistry
and Physics
Discussions

1   Introduction

Mineral dust is one of the major types of tropospheric aerosols in the atmosphere
(Arimoto et al., 2006; Ramanathan et al., 2001). Mineral dust has a profound impact on
the radiative balance of the Earth by scattering and absorbing solar radiation (Huang et

5   al., 2010; Wang et al., 2010; Huang et al., 2014; Li et al., 2016); this dust can also act
as cloud condensation nuclei (CCN) to alter the precipitation rate and hydrological
cycle of the Earth (Rosenfeld et al., 2001). East Asia includes the Taklimakan, Tengger,
Badain Jaran and Gobi Deserts and is thus considered to be one of the major source
regions of natural dust in the world, as it produces large amounts of natural mineral dust

10   (Zhang et al., 1997; Wang et al., 2008; Che et al., 2011, 2013; Ge et al., 2014; Xin,
2005, 2010, 2015). Once dust aerosols are lifted into the atmosphere by strong surface
winds, they can be transported up to thousands of kilometres away from their source
regions (Chen et al., 2013; Liu et al., 2015; Huang et al., 2008). The long-range
transport of tropospheric aerosols from their dust source regions in East Asia plays a

15   key role in aerosol radiative forcing (Ge et al., 2011). For instance, Washington et al.
(2003) demonstrated that there is large-scale uncertainty associated with the estimation
of radiative forcing caused by dust particles, which is mainly due to their non-sphericity
and chemical composition. Compared to natural mineral dust, black carbon (BC), which
is generated from the incomplete combustion of fossil fuels and biomass burning, is

20   also a major anthropogenic pollutant. Numerous modelling studies have
demonstrated the importance of BC in regional climate change (Ramanathan et
al., 2005; Menon et al., 2002). Therefore, the largest source of uncertainty in

Atmospheric
Chemistry
and Physics
Discussions

determining global radiative forcing is the quantification of the direct and indirect

effects of mineral dust and other anthropogenic aerosols (IPCC, 2013).

Recently, the potential impacts of anthropogenic soil dust have also received an

increasing amount of attention (Prospero et al., 2002; Huang et al., 2015a; Tegen and

5   Fung, 1995; Tegen et al., 2002; Shi et al., 2015; Pu et al., 2015; Wang et al., 2015).

Anthropogenic mineral dust can also influence air quality and human health through

the processes of their emission, transport, removal, and deposition (Aleksandropoulou

et al., 2011; Chen et al., 2013; Huang et al., 2014, 2015a, 2015b; Kim et al., 2009; Li

et al., 2009; Mahowald and Luo, 2003; Zhang et al., 2005, 2015). Ginoux et al. (2010)

10   estimated that anthropogenic dust accounts for 25% of all dust aerosols using

observational data from MODIS (Moderate Resolution Imaging Spectroradiometer)

Deep Blue satellite products combined with a land-use fraction dataset. Anthropogenic

dust primarily originates from urban and regional sources, especially during the winter;

this dust is commonly enriched in heavy metals and other toxic elements (Kamani et

15   al., 2015; Li et al., 2013; Wang et al., 2015; Zhang et al., 2013). Northeastern China

and its surrounding regions are generally regarded as industrial areas that are most

strongly affected by human activities. Because anthropogenic dust emissions from

disturbed soils are not well constrained, we define anthropogenic dust as mineral dust

from areas that have been disrupted by human activities, such as deforestation,

20   overgrazing, and agricultural and industrial activities (Aleksandropoulou et al., 2011;

Tao et al., 2014, 2015, 2017; Tegen and Fung, 1995; Tegen et al., 2002, 2004;

Thompson et al., 1988); anthropogenic dust is thus different than natural mineral dust,

which originates from desert regions (Che et al., 2011, 2013; Goudie and Middleton, 2001; Li et al., 2012; Park and Park, 2014; Pu et al., 2015; Wang et al., 2008, 2010). This assumption is consistent with the results of a recent study by Huang et al. (2015a), who found that anthropogenic dust comprises 91.8% of regional emissions in eastern

5 China and 76.1% of regional emissions in India (e.g., Figure 10 in Huang et al., 2015a). This may be due to the larger population densities of eastern China and India, which are characterized by intense human activity (Huang et al., 2015a; Wang et al., 2013). Understanding the microphysical and optical properties of natural dust mixed with the other atmospheric aerosols produced by human activities in the troposphere has a

10 critical impact on our ability to predict atmospheric compositions and global climate change (Nie et al., 2014; Ramanathan et al., 2007; Spracklen and Rap, 2013). Several attempts have been made to investigate the significance of the effects of dust on global climate, meteorology, atmospheric dynamics, ecosystems and human health (Rosenfeld et al., 2011; Qian et al., 2004). Limited field campaigns have focused on the properties

15 of natural dust and anthropogenic aerosols, especially those of the anthropogenic dust aerosols produced by human activities near dust source regions. In this paper, we focus on the measured optical and microphysical properties of natural dust and anthropogenic aerosols. This paper presents detailed emission information obtained from measurements made in Wuwei, Zhangye, and Dunhuang over Northwestern China from

20 3 April to 16 May in 2014 in order to better understand the sources of regional emissions and the mixing state of air pollution with mineral dust. We also used statistical analysis

to identify the possible signatures of natural dust storms transported from dust source regions.

2   Methodology

2.1   Measurement Site

5   The dust field campaign was carried out along the Hexi Corridor from 3 April to 16 May 2014. A ground-based mobile facility of the Semi-Arid Climate and Environment Observatory of Lanzhou University (SACOL) for Energy Atmospheric Radiation Measurements was used in three sites, which are located in Wuwei (37.72°N, 102.89°E; 3 - 7 April), Zhangye (39.04°N, 100.12°E; 9 - 28 April), and Dunhuang (39.96°N,

10   94.33°E; 3 - 16 May). The locations of these sites are shown in the top panel of Figure 1. The Hexi Corridor is considered to be a heavily polluted area because of the combination of local topography and the human activities occurring over Northwestern China. As shown in the bottom panels of Figure 1, the site in Wuwei is located only ~17 km away from the Tengger Desert and ~20 km away from the Qilian Mountains;

15   therefore, anthropogenic air pollutants originating from Wuwei City can directly influence the sampling site because of the prevailing wind direction along the local topography. The land surface type in Linze farmland in Zhangye (LFZ) is similar with Wuwei (Figure 2b). However, the sampling site in Dunhuang was located approximately 30 km away from the urban area and in the upwind direction of

20   Dunhuang, and the primary components in Dunhuang were dominated by natural mineral dust (Figure 2c). As shown in Figure 2a and 2b, the local tropospheric aerosols

in Wuwei and Zhangye were dominated by anthropogenic soil dust due to agricultural

cultivation activity (e.g., land planning, ploughing, and disking), especially during the

floating dust period.

2.2 Instrumentation

5   Automatic measurements of ambient temperature, relative humidity, pressure, wind

direction, and wind speed were collected at 1-min intervals based on the microphysical

and optical parameters of aerosols described above. Finally, all datasets measured

during this field campaign were adjusted to standard temperature and pressure

conditions (STP; T=273.15 K, P=101.325 kPa). We also measured aerosol absorption

10   and scattering coefficients, mass concentrations, and aerosol number size distribution

during the 2014 dust field campaign, in which 5-min averaged data were used. The

wind direction datasets are associated with the aerosol absorption and scattering

coefficients and can be used to determine the origins of natural and anthropogenic dust.

Figure 3a shows the ground-based mobile laboratory used in Dunhuang during the dust

15   field campaign along the Hexi Corridor over Northwest China. A sampler inlet was

installed at the top of the ground-based mobile laboratory, using 1 μm and 2.5 μm

impactors for different instruments, which are shown in Figure 3b. All of the collectors

were operated at 50°C to dry the aerosols (i.e., to a relative humidity (RH) of less than

40%). The mass concentration of $PM_{2.5}$ was measured continuously using an R&P

20   1400a analyser, which is based on the principle of tapered element oscillating

microbalance (TEOM), with a flow rate of 16.7 L min^{-1}. To compare the properties of

coarse and fine mode particles, two integrating nephelometers (TSI Model 3563) with

1 μm and 2.5 μm impactors were employed to measure aerosol scattering coefficients

(σ_{sp}) at 450, 550, and 700 nm; the detection limits of these instruments were 0.44×10

Mm^{-1}, 0.17×10 Mm^{-1}, and 0.26×10 Mm^{-1}, respectively, and the instruments had a

5   signal-to-noise ratio (S:N) of 2:1 (Anderson et al., 1996; Shi et al., 2013). Then, a multi-

angle absorption photometer (MAAP-5012) was used to measure aerosol absorption

coefficients (σ_{ap}) at 670 nm. The particle size distribution ranging from 0.5–20 μm was

measured using an aero-dynamical particle sizer (APS-3321), assuming that all aerosols

are homogeneous and spherical particles, despite the fact that the observed coarse mode

10   dust particles exhibit non-spherical geometries (Mishchenko et al., 1995). The mass

absorption coefficient (MAC, hereinafter α) is a key parameter that can be used to

attribute the light absorption of aerosols to BC and to understand its effects on climate.

The MAC values of BC span a wide range in the literature. For instance, the MAC of

BC has been defined as 7.5 m^2 g^{-1} at 550 nm and 12–13 m^2 g^{-1} at ~350 nm (Adler et al.,

15   2010); these values are calculated by assuming that the imaginary part of the complex

refractive index (RI) of BC is independent of the wavelength (λ) (Bond and Bergstrom,

2006). To calculate the aerosol absorption coefficient (σ_{ap}), the following equation is

used:

$$\sigma_{ap} = \alpha \times m_{BC} \qquad (1)$$

20   where $\alpha = 6.6$ m^2 g^{-1} and m_{BC} is the mass concentration of BC.

The wavelength-dependent variation of σ_{sp} is characterized by the scattering

Ångström exponent (SAE, $Å_{sp}$), which is defined as:

Atmospheric
Chemistry
and Physics
Discussions

$$\mathring{A}_{sp}(\lambda_1/\lambda_2) = -\frac{\ln(\sigma_{sp,\lambda_1}/\sigma_{sp,\lambda_2})}{\ln(\lambda_1/\lambda_2)} \qquad (2)$$

where σ_{sp,λ_1} and σ_{sp,λ_1} are the aerosol scattering coefficients at wavelengths λ_1 and λ_2, respectively. In this paper, we calculated $\mathring{A}_{sp}$ from 450–700 nm (i.e., from $\sigma_{sp,450}$ and $\sigma_{sp,700}$).

5   The attribution of observed atmospheric light absorption to BC is an important step in understanding the overall climate effects of aerosols. Some studies have attempted to perform this attribution based on the assumption of the wavelength dependence of absorption (e.g. Favez et al., 2009; Yang et al., 2009). It is often assumed that the imaginary RI of BC is independent of wavelength (λ) and that the absorption cross-

10   section of BC varies as λ^{-1} (Bond and Bergstrom, 2006).

To calculate the single scattering albedo (ω) at 550 nm, we first adjust the σ_{ap} values from 670 to 550 nm; this equation is listed as follows:

$$\sigma_{ap,550} = \sigma_{ap,670} \times \left(\frac{\lambda_{670}}{\lambda_{550}}\right)^{AAE} \qquad (3)$$

where λ is wavelength and the absorption Ångström exponent (AAE) corresponds to

15   the λ^{-1} dependence of the absorption of BC, which is typically assumed to be AAE=1. However, we note that the actual AAE of BC can be greater or less than 1, as this value is highly dependent on the internal/external core size and its ageing process (Gyawali et al., 2009).

The single scattering albedo is a key parameter that can be used to investigate the

20   microphysical and optical properties of atmospheric aerosols. The single scattering albedo is defined as the ratio of the scattering coefficient to the total extinction coefficient (i.e., the scattering + absorption coefficients) at 550 nm using Eq. (4):

$$\omega_{550} = \frac{\sigma_{sp}}{\sigma_{ap}+\sigma_{sp}} \qquad (4)$$

The parameter of mass scattering efficiency (MSE) is calculated as the slope of the

RMA linear regression of $\sigma_{sp}^{2.5}$ and PM$_{2.5}$, which is calculated using Eq. (5):

$$MSE = \frac{\sigma_{sp}^{2.5}}{PM_{2.5}} \qquad (5)$$

5   where $\sigma_{sp}^{2.5}$ is the aerosol scattering coefficient at 550 nm and PM$_{2.5}$ is the mass

concentration of atmospheric aerosols with size diameters of less than 2.5 μm.

3   Results

During this dust field campaign, four floating dust episodes (which are shown as dotted

boxes in Figure 4) occurred on 3–7 April in Wuwei and on 9–12, 14–15 and 25–28

10   April in Zhangye. We also observed the microphysical and optical properties of natural

mineral dust during a heavy dust storm (shown as a solid box in Figure 4) from 23 to

25 April 2014. According to the land surface types shown in Figure 2, one of the major

aims of this study is to investigate the characteristics of anthropogenic and natural dust,

which are present in floating dust episodes and dust storms, respectively, and represent

15   the fine mode soil dust that is produced by agricultural cultivations and the coarse mode

mineral dust that originates from desert regions, respectively. Therefore, significant

differences in the optical and microphysical properties of these aerosols were observed

under different atmospheric conditions (e.g., dust storms, floating dust episodes and

background conditions). Figure 4 illustrates the temporal variations in σ_{ap}, σ_{sp}, ω

20   and MSE at 550 nm as well as those in Å$_{sp}$ (calculated from 450 nm to 700 nm) and

aerosol size distribution in Wuwei, Zhangye, and Dunhuang from 3 April to 16 May

2014. These surveys were conducted in Wuwei, Zhangye, and Dunhuang in chronological order, as is illustrated in Figure 4. The statistical analyses of the optical parameters measured during this dust field campaign are summarized in Table 1 (hereinafter, these results are given as the mean $\pm$ the standard deviation of the 5-min

5 averaged datasets). One of the most significant features in Figure 4a is that the variation of $\sigma_{sp}^{2.5}$ is highly consistent with that of $\sigma_{sp}^{1.0}$ during the field campaign. The values of $\sigma_{sp}^{1.0}$ and $\sigma_{sp}^{2.5}$ are very close in Wuwei and Zhangye; however, the large differences observed in Dunhuang indicate that fine mode particles dominate the scattering coefficient in farmland regions, whereas coarse mode particles play a more important

10 role closer to the desert regions of Dunhuang. Except for the values obtained during a heavy dust storm in Zhangye, the $\sigma_{sp}^{2.5}$ values measured at 550 nm using the nephelometer range from ~50–429 Mm^{-1} and ~20–532 Mm^{-1} at Wuwei and Zhangye, respectively, which can be compared to the $\sigma_{ap}^{2.5}$ values of ~3.6–69.6 Mm^{-1} and ~1.3– 64.5 Mm^{-1} measured at Wuwei and Zhangye, respectively. The lowest value of $\sigma_{ap}^{2.5}$

15 obtained during the field campaign (i.e., 2.7 ± 1.2 Mm^{-1}) was collected in Dunhuang. This observation reveals that natural mineral dust is still a weaker absorber than anthropogenic soil dust that has been mixed with air pollutants (e.g., BC). Values of ω_{550} were estimated using the aerosol scattering coefficient obtained from the nephelometer and the aerosol absorption coefficient of the MAAP at 550 nm, with a

20 nominal instrumental uncertainty of $\pm$ 0.02. Compared with Figure 4a, Figure 4b indicates that the majority of ω_{550} values are much higher in Dunhuang than they are in the other two sites; these values range from ~0.80 to 0.99, with a mean value of

0.95 ± 0.02. Similar results were also found in Zhangye during the dust storm because

of the presence of coarse mode particles. However, only 0.7% and 21.9% of the values

of ω_{550} reach up to 0.95 in Wuwei and Zhangye (Figure 7), and their average ω_{550}

values are much lower (0.91 ± 0.03 and 0.93 ± 0.04, respectively) and exhibit larger

5   variation than those in Dunhuang. This phenomenon most likely indicates that natural

dust aerosols are dominant in Dunhuang, since mineral dust scatters more and absorbs

less than other atmospheric aerosols. Figure 4c reveals that the $Å_{sp}$ values of aerosols

with diameters of less than 1 μm ($Å_{sp}^{1.0}$) are much higher than those of $Å_{sp}^{2.5}$ and that

$Å_{sp}$ values decrease significantly from Wuwei to Dunhuang. The average MSE values

10   in Wuwei, Zhangye and Dunhuang are 2.8 ± 0.7 m^2 g^{-1}, 2.2 ± 0.8 m^2 g^{-1} and 1.5 ± 0.7

m^2 g^{-1}, respectively, which have 5-min maximum values of 6.3 m^2 g^{-1}, 9.5 m^2 g^{-1}, and

8.5 m^2 g^{-1}, respectively. The higher MSE values in Wuwei and Zhangye reflect the fact

that anthropogenic dust, which is influenced by local soil dust during floating dust

episodes, scatters more solar radiation than natural dust (Figure 4d). Figure 4e indicates

15   that fine mode particles that are less than 1 μm in diameter are dominant in Wuwei and

Zhangye, except during a strong dust storm that occurred in Zhangye on 23–25 April

2014. Although the number concentration of fine mode particles is also higher than that

of coarse mode particles in Dunhuang, the average percentage of coarse mode particles

relative to total atmospheric particles is 55%, which is higher than the relative

20   percentages observed in Wuwei and Zhangye. On 23–25 April 2014, a severe dust

storm occurred in Zhangye, along with a strong northerly wind. The 5-min average

$\sigma_{sp}^{2.5}$ value at 550 nm increased to 5813 Mm^{-1}, which is ~10 times higher than that

measured in non-dust plume periods in Zhangye (532 Mm^{-1}), while the maximum value

of $\sigma_{ap}^{2.5}$ was 59.6 Mm^{-1} during this dust storm, which is slightly lower than that

measured during non-dust plume periods (64.5 Mm^{-1}). Figures 4b and 4c indicate that

the peaks of ω_{550} (>0.99) that are associated with the lowest values of Å$_{sp}$ are close

5   to those observed in another field campaign that studied dust dominant particles in

Northwestern China (Li et al., 2010). Figure 4e demonstrates that the number

concentration of coarse mode particles with diameters of 1–5 μm is higher than 900

cm^{-3}, which indicates that pure coarse mode particles from desert regions are dominant

during dust storms in Zhangye. These results are consistent with those of a previous

10   study, in which the aerosol diameter (De) of PM$_{10}$ was determined to be larger during

dust plume periods than it was during non-dust plume periods (Wang et al., 2010).

Here, we also present the diurnal cycles of $\sigma_{sp}^{2.5}$, $\sigma_{sp}^{1.0}$, $\sigma_{ap}^{2.5}$, and ω_{550}, as well as those

of the Å$_{sp}$ and MSE values in Wuwei (red line), Zhangye (black line), and Dunhuang

(blue line) throughout these periods (Figure 5). As shown in Figure 5a and 5b, the

15   values of $\sigma_{sp}^{2.5}$, $\sigma_{sp}^{1.0}$ and $\sigma_{ap}^{2.5}$ at 550 nm present bimodal distributions in Wuwei and

Zhangye, which are consistent with the variations in ω_{550} (Figure 5e). The average

values of $\sigma_{sp}^{2.5}$, $\sigma_{sp}^{1.0}$ and $\sigma_{ap}^{2.5}$ in Dunhuang are 53 Mm^{-1}, 25 Mm^{-1} and 2.6 Mm^{-1},

respectively, which are much lower than those measured in Wuwei and Zhangye

(Figure 5a and 5b). The highest values of $\sigma_{ap}^{2.5}$ indicate that not only anthropogenic

20   mineral dust but also local air pollutants (e.g., BC and OC) were found in these regions;

these pollutants originated from biomass and the burning of fossil fuels. Compared with

the lower ω_{550} values that occurred at ~8:00 and ~20:30 LST in Wuwei and Zhangye,

the presence of only slight variations in ω_{550} in Dunhuang indicates that coarse mode

particles (e.g., natural dust aerosols) are dominant in Dunhuang (Figure 5e).

Additionally, a comparison of the Å$_{sp}$ values due to fine mode and coarse mode particles

that are less than 1 μm and 2.5 μm in size, respectively, indicates that there are large

5   variations in $\text{Å}_{sp}^{2.5}$ and $\text{Å}_{sp}^{1.0}$ in Wuwei, ranging from ~1.0–1.7 and ~1.8–2.3,

respectively. The lowest values of $\text{Å}_{sp}^{2.5}$ and $\text{Å}_{sp}^{1.0}$ observed in Dunhuang also suggest

that its atmospheric aerosols are dominated by coarse mode particles (Figure 5c-5d).

Another feature is that the $\text{Å}_{sp}^{1.0}$ value of fine mode particles is significantly higher than

that of $\text{Å}_{sp}^{2.5}$. Large variations in MSE are found at all three sites; MSE values are

10   highest during the floating dust episodes in Wuwei and lowest in Dunhuang because of

the amounts of pure coarse mode particles that are present during background surface

conditions (Figure 5f). Diurnal variations in the aerosol number distribution (hereinafter

defined as dN/dlogD$_p$) in the range of 0.5 μm ≤ D$_p$ (particle diameter) ≤ 5 μm were

also observed using the aerodynamic particle sizer (APS) instrument (Figure 6). As is

15   shown in Figure 6a, the accumulated fine mode particles (<1 μm) increased in Wuwei,

yielding a maximum number distribution of more than 300 cm^{-3} due to the frequent

outbreaks of floating dust episodes that occurred in Wuwei on 3–7 April 2014. The

similar patterns of fine mode particles imply that Wuwei has very similar pollutant

emission sources as Zhangye, but with a slightly lower number distribution of fine mode

20   particles, as is shown in Figure 6b. We suggest that the fine mode particles represent

the dominant contributions in Wuwei and Zhangye, which is due to the formation of

local anthropogenic soil dust by agricultural cultivations. However, large differences

Atmospheric
Chemistry
and Physics
Discussions

are found in Dunhuang because of its higher percentage of coarse mode particles relative to total atmospheric particles; this region yields 5-min average values of 203 ± 125 cm^{-3} and 234 ± 248 cm^{-3} for fine mode and coarse mode particles, respectively (Figure 6c).

5   Figure 7 shows the histograms of the single scattering albedo values observed at 550 nm from 3 April to 16 May 2014. During the floating dust period in Wuwei, the majority of the ω_{550} values of fine mode particles that originated from anthropogenic soil dust range from ~0.90–0.93; approximately 10%–20% of those values range from ~0.88–0.90 and ~0.93–0.95. The overall range of ω_{550} values observed in Zhangye is similar

10   to that observed in Wuwei. The ω_{550} values that range from ~0.90–0.93 are 30% higher than those in Zhangye. This observation indicates that the atmospheric aerosols not only include anthropogenic soil dust that is smaller than 1 μm but also have undergone mixing with air pollutants (e.g., BC) during their transportation from urban and industrial regions. This result is consistent with that of Li et al. (2010), who noted

15   that the SSA of a dust storm was approximately 0.98 for coarse mode particles, while lower SSA values (i.e., ranging from 0.89 to 0.91) were closely related to local air pollution. Thus, we infer that the occurrence of much lower ω_{550} values in Wuwei and Zhangye than in Dunhuang is due to the mixing of anthropogenic pollutants with local mineral dust. However, the ω_{550} values in Dunhuang range from ~0.93–0.98,

20   with the majority of these values falling between ~0.95–0.98 because of the high percentage of coarse mode particles. These results are consistent with that of a previous study, which indicated that the surface measurement of SSA for coarse mode particles

Atmospheric
Chemistry
and Physics
Discussions

from Saharan desert regions at 550 nm yielded a value of 0.97 ± 0.02 (Cattrall et al.,

2003). Additionally, the wind roses in Figure 8 can be used to provide further insights

into the correlation between meteorology and the aerosol scattering (absorption)

coefficients. The wind direction accompanying $\sigma_{sp}^{2.5}$ and $\sigma_{ap}^{2.5}$ at 550 nm most likely

5   represents the emissions from both local sources and regional transport from remote

regions. The dominant wind direction is generally more abundant to the west. Figures

8a and 8b indicate that the higher values of $\sigma_{sp}^{2.5}$ are found along with the northwest

wind, while the majority of $\sigma_{ap}^{2.5}$ values are dominated by the southeast wind because

of the emissions of anthropogenic pollutants from the city centre of Wuwei. However,

10   the fact that the highest values of $\sigma_{sp}^{2.5}$ and $\sigma_{ap}^{2.5}$ are associated with the western wind

in Zhangye most likely indicates that these emissions originate from both anthropogenic

soil dust and air pollutants from their upwelling regions (Figure 8c and 8d). However,

both $\sigma_{sp}^{2.5}$ and $\sigma_{ap}^{2.5}$ were probably influenced by coarse mode mineral dust due to the

presence of northwest wind in Dunhuang (Figure 8e and 8f).

15   MSE is a key parameter that can be used to estimate the radiative forcing effects due to

atmospheric particles on global climate. Therefore, several studies have been performed

to determine the optical properties of aerosols using MSE values (Laing et al., 2016).

For instance, Hand and Malm (2007) noted that the MSE is mainly dependent on

particle composition (e.g., the particle refractive index and aerosol size distribution).

20   As shown in Figure 9a, coarse mode particles have significantly higher ω_{550} (>0.93)

and lower MSE (1< MSE<2) values because of the presence of natural mineral dust

under background weather conditions in Dunhuang. However, there appears to be no

clear difference between the ω_{550} and MSE values due to floating dust periods in Wuwei and Zhangye. The presence of lower and higher MSE values in Wuwei and Zhangye, respectively, suggests that fine mode particles can not only be attributed to floating dust periods (due to local soil dust) but also include BC, OC and other air

5   pollutants that originated from the burning of biomass and fossil fuels. For instance, the large variations in ω_{550} (~0.71–0.95 and ~0.68–0.99, respectively) and MSE (~0.9– 6.3 $m^2 \, g^{-1}$ and ~0.4–9.5 $m^2 \, g^{-1}$, respectively) observed in Wuwei and Zhangye are consistent with values that were previously measured during dust storms or biomass burning events (Li et al., 2010; Laing et al., 2016). Another notable feature is the

10   remarkable discrepancy between the optical properties of aerosols for a given type of aerosol with diameters of less than 1 μm and 2.5 μm. Although the values of $\sigma_{sp}^{1.0}$ measured during this dust field campaign are only slightly lower than those of $\sigma_{sp}^{2.5}$ (as is indicated in Figures 9b and 9c), the $\text{Å}_{sp}^{1.0}$ values range from ~1.1–2.4 (mean: 2.1) for fine mode particles because of floating dust episodes in Wuwei, compared to the values

15   of ~0.2–1.7 (mean: 1.3) observed during the same period in Wuwei. Similar results are also found at the other two sites in Zhangye and Dunhuang.

The microphysical and optical properties of aerosols observed during this dust field campaign are summarized in Figure 10. The boxes and whiskers denote the 10th, 25th, median, 75th, and 90th percentiles of the data, with dots marking their average values.

20   We determined that the values of both σ_{sp} and σ_{ap} at 550 nm are higher in Wuwei during floating dust episodes than that in Zhangye and Dunhuang during background conditions. The average values of $\sigma_{sp}^{1.0}$, $\sigma_{sp}^{2.5}$, and $\sigma_{ap}^{2.5}$ measured at 550 nm during

Atmospheric
Chemistry
and Physics
Discussions

this field campaign in Wuwei are 75 ± 29 Mm^{-1}, 102 ± 40 Mm^{-1}, and 11.5 ± 7.8 Mm^{-1}, respectively. The 90th percentage of $\sigma_{sp}^{2.5}$ in Zhangye is due to the dust storm that occurred on 23–25 April 2014. However, the highest ω_{550} value is found in Dunhuang and is due to the presence of coarse mode particles during background conditions. We

5   note that there are large differences in Å$_{sp}$ between fine mode and coarse mode particles. The average values of Å$_{sp}^{2.5}$ and Å$_{sp}^{1.0}$ are 1.3 ± 0.3 and 2.1 ± 0.2 during floating dust episodes in Wuwei, respectively, whereas those in Dunhuang are 0.5 ± 0.3 and 0.9 ± 0.4, respectively. The highest MSE in Wuwei and the lowest MSE in Dunhuang indicate that fine mode mineral dust particles scatter more solar radiation than coarse

10   mode particles. Aerosol optical depth (AOD) is a major optical parameter for aerosol particles and is a key factor affecting global climate (Holben et al., 1991, 2001, 2006; Srivastava and Bhardwaj, 2014). AOD can not only represent local air pollution but can also be used to observe dust storms. For instance, Dubovik et al. (2002) demonstrated that non-spherical mineral dust can be retrieved using the assumption of spherical

15   aerosols for high aerosol loading (AOD >0.5, Å <0.7) in desert regions due to dust events. Figure 11 illustrates the spatial distribution of deep blue AOD at 550 nm in East Asia retrieved using Terra MODIS during a heavy dust storm over northern China on 24 April 2014. During this dust storm, the spatial distribution of high aerosol loadings with AOD values of >1.6 over Northwest China was observed; in this distribution, the

20   transport of natural mineral dust from the Taklimakan Desert to the downwelling regions over China can be clearly seen. The most prominent feature in Figure 12 is that $\sigma_{sp}^{2.5}$ reaches its peak value from ~209 Mm^{-1} to 5813 Mm^{-1} and that a strong relationship

Atmospheric
Chemistry
and Physics
Discussions

(R^2=0.91) existed between $\sigma_{sp}^{2.5}$ and $\sigma_{ap}^{2.5}$ during the dust storm on 23–25 April 2014.

However, the values of $\sigma_{ap}^{2.5}$ observed during the dust storm are consistent with those

measured during floating dust episodes in Wuwei and Zhangye. Therefore, we note that

large differences in $\sigma_{sp}^{2.5}$ are found between natural and anthropogenic mineral dust

5   because of the presence of fine mode and coarse mode particles during floating dust

episodes and dust storms, but that they record similar ranges of $\sigma_{ap}^{2.5}$. We also observed

the lowest values of $\sigma_{ap}^{2.5}$ and $\sigma_{sp}^{2.5}$ (which range from ~0.9–13.1 and ~14–264 Mm^{-1},

respectively) in Dunhuang on 3–16 May, which indicates that natural mineral dust

represents the dominant particles under background conditions. The observed higher

10    $\sigma_{ap}^{2.5}$ and lower $\sigma_{sp}^{2.5}$ values suggest that fine mode anthropogenic dust particles were

dominant in Wuwei and Zhuangye during floating dust episodes, in contrast to the

coarse mode particles observed during the dust storm in Dunhuang.

Figure 13 shows the average aerosol number size distribution observed using the APS

instrument during this field campaign. These data clearly show that the dominant

15   particles during the dust storm in Zhangye are coarse mode particles ranging in size

from 1 μm to 5 μm, which reach a maximum value of 596 cm^{-3} at a size of 1.60 μm.

Compared with dust storms, the value of dN/dlogD$_p$ reaches a peak with values of ~335

cm^{-3} and ~345 cm^{-3} at 0.67 μm during typical floating dust episodes on 4–7 and 9–15

April 2014, respectively. This observation indicates that fine mode anthropogenic soil

20   dust mixed with local air pollutants was dominant during floating dust episodes on 3–

7 and 9–15 April 2014 in Wuwei and Zhangye. However, another floating dust episode

that occurred in Zhangye reveals a bimodal variation of dN/dlogD$_p$ at 0.67 μm and 1.49

μm. It also should be noted that the lowest value of dN/dlogD$_p$ for fine mode particles was observed in Dunhuang because of the background weather conditions. These results are very close to those of previous studies that stated that atmospheric particles were dominated by both anthropogenic soil dust and air pollutants during floating dust

5   episodes; however, the amount of coarse mode particles increased sharply during natural dust storms that originated from dust source regions (Wang et al., 2010; Li et al., 2010).

4   Conclusions

To determine the optical and microphysical properties of atmospheric particles in

10   anthropogenic soil dust and natural mineral dust, a ground-based mobile laboratory was deployed near the dust source regions along the Hexi Corridor over Northwest China from 3 April to 16 May 2014. Two of the sampling sites were located in farmland areas in Wuwei and Zhangye, and the other site was located near the edge of the Gobi Desert in Dunhuang. Therefore, the land surface types in Wuwei and Zhangye represent

15   anthropogenic soil dust generated by human activities (e.g., ploughing, coal combustion from domestic use, and biomass burning), while the land surface type in Dunhuang represents mineral dust.

During this dust field experiment, which was performed from April to May 2014, four floating dust episodes and one dust storm episode were observed in Wuwei and

20   Zhangye. There are two major findings observed in this study. The most prominent conclusion is that there are significant differences in the optical and microphysical

properties of aerosols between anthropogenic soil dust and natural mineral dust under

different atmospheric conditions (e.g., dust storms, floating dust episodes and

background conditions). For instance, the average values of $\sigma_{sp}^{2.5}$, $\sigma_{ap}^{2.5}$, ω_{550} at 550

nm, $\mathring{A}_{sp}^{2.5}$, MSE and dN/dlogD$_p$ are 183 Mm^{-1}, 6.9 Mm^{-1}, 0.91, 0.9, 2.4 m^2 g^{-1} and 2072

5   cm^{-3}, respectively, during floating dust periods, whereas these values are 1108 Mm^{-1},

13.5 Mm^{-1}, 0.99, -0.02, 1.7 m^2 g^{-1}, and 9923 cm^{-3}, respectively, during dust storms. The

number concentrations of coarse mode particles with diameters of 1–5 μm can reach a

peak of 900 cm^{-3}, which reveals that pure coarse mode particles from desert regions

were dominant during dust storms in Zhangye. However, the overall variations in ω_{550},

10   which ranges from 0.71 to 0.95 and 0.64 to 0.98 during floating dust episodes in Wuwei

and Zhangye, respectively, indicate that atmospheric aerosols not only include

anthropogenic soil dust that is smaller than 1 μm but has also undergone mixing with

air pollutants (e.g., BC) because of their transportation from urban and industrial

regions. In addition to the large discrepancies between fine mode and coarse mode

15   particles observed under different weather conditions, there are also significant

differences between the optical and microphysical properties of the given atmospheric

particles that are smaller than 1 μm and 2.5 μm. We note that the values of $\sigma_{sp}^{1.0}$

$(75 \pm 29$ Mm$^{-1})$ are only slightly lower than those of $\sigma_{sp}^{2.5}$ $(102 \pm 40$ Mm$^{-1})$ that are

observed in Wuwei. However, there are significant differences between the values of

20   $\mathring{A}_{sp}^{1.0}$ and $\mathring{A}_{sp}^{2.5}$, which range from ~1.1–2.4 (mean: 2.1) and ~0.2–1.7 (mean: 1.3),

respectively, because of the occurrence of floating dust episodes in Wuwei.

During the heavy dust storms studied here, atmospheric aerosols sharply increased

because of the addition of coarse mode particles ranging in diameter from 1–5 μm. The

maximum $dN/dlogD_p$ value for coarse mode particles reached 596 cm^{-3} at 1.60 μm,

which is 5 times higher than that observed at the same site under background weather

conditions. However, $dN/dlogD_p$ reached its peak values of 335 cm^{-3} and 345 cm^{-3} for

5   fine mode particles at 0.67 μm during floating dust events in Wuwei and Zhangye,

respectively. These results indicate that these atmospheric aerosols not only were

dominated by anthropogenic soil dust produced by agricultural cultivations but also

underwent mixing with local air pollutants because of the burning of biomass and coal.

These results are very similar to those of previous studies, which indicated that

10   atmospheric particles were dominated by both anthropogenic soil dust and air pollutants

during floating dust events but that natural mineral dust due to dust storms originated

from dust source regions.

5   Data availability

All data sets and codes used to produce this study can be obtained by contacting Xin

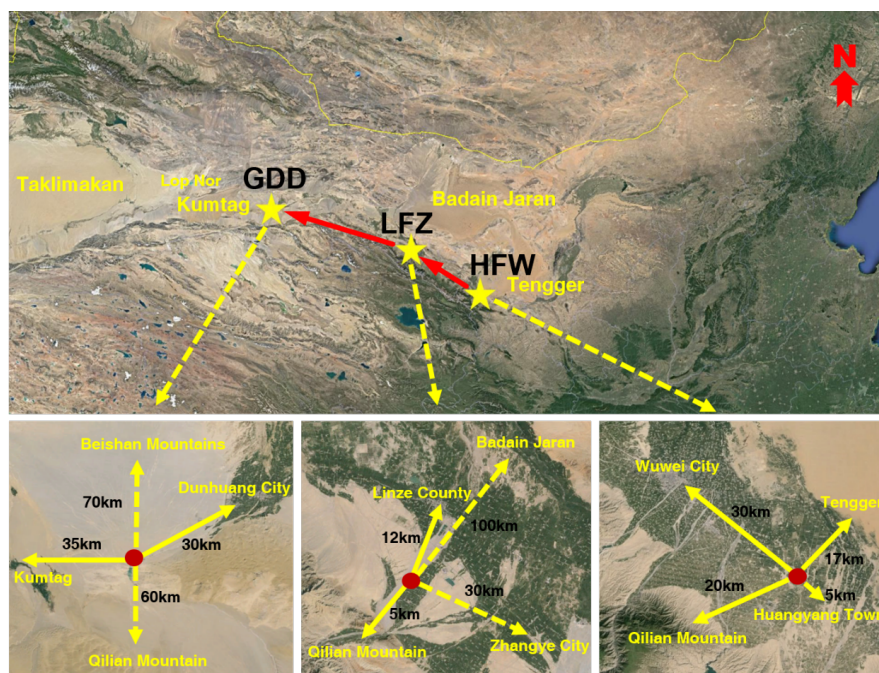15   Wang (wxin@lzu.edu.cn).The MODIS data used in this study are available at Aerosol

Product, https://modis.gsfc.nasa.gov/data/dataprod/mod04.php.

Competing interests. The authors declare that they have no conflict of interest.

Atmospheric
Chemistry
and Physics
Discussions
Open Access

Figure 1. The sampling locations of ground-based mobile laboratory and their surrounding areas near dust source regions during the 2014 dust field campaigns at **(a)** Huangyang Farmland in Wuwei (HFW, 37.72°N, 102.89°E; 1691 m a.s.l.), **(b)** Linze Farmland in Zhangye (LFZ, 39.04°N, 100.12°E; 1578 m a.s.l.) and **(c)** Gobi Desert in Dunhuang (GDD, 39.96°N, 94.33°E; 1367 m a.s.l.).

Atmospheric
Chemistry
and Physics
Discussions
Open Access
EGU
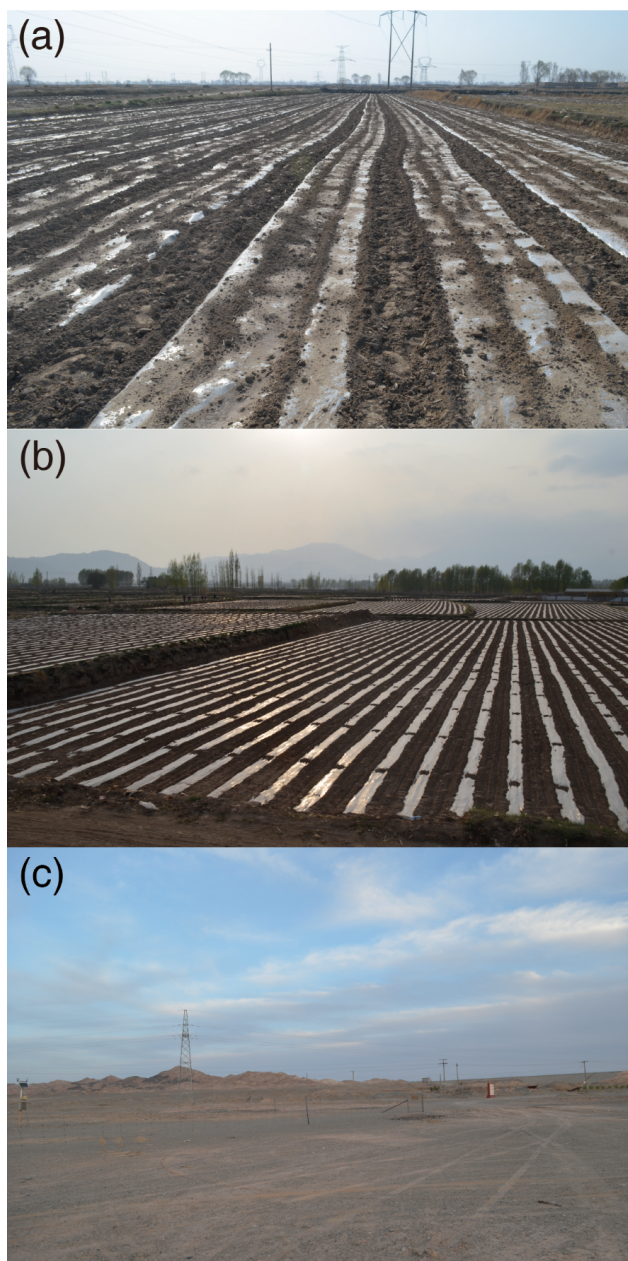
Figure 2. Same as **Figure 1** but for land surface conditions at **(a)** Huangyang Farmland in Wuwei (HFW), **(b)** Linze Farmland in Zhangye (LFZ), and **(c)** Gobi Desert in Dunhuang (GDD).
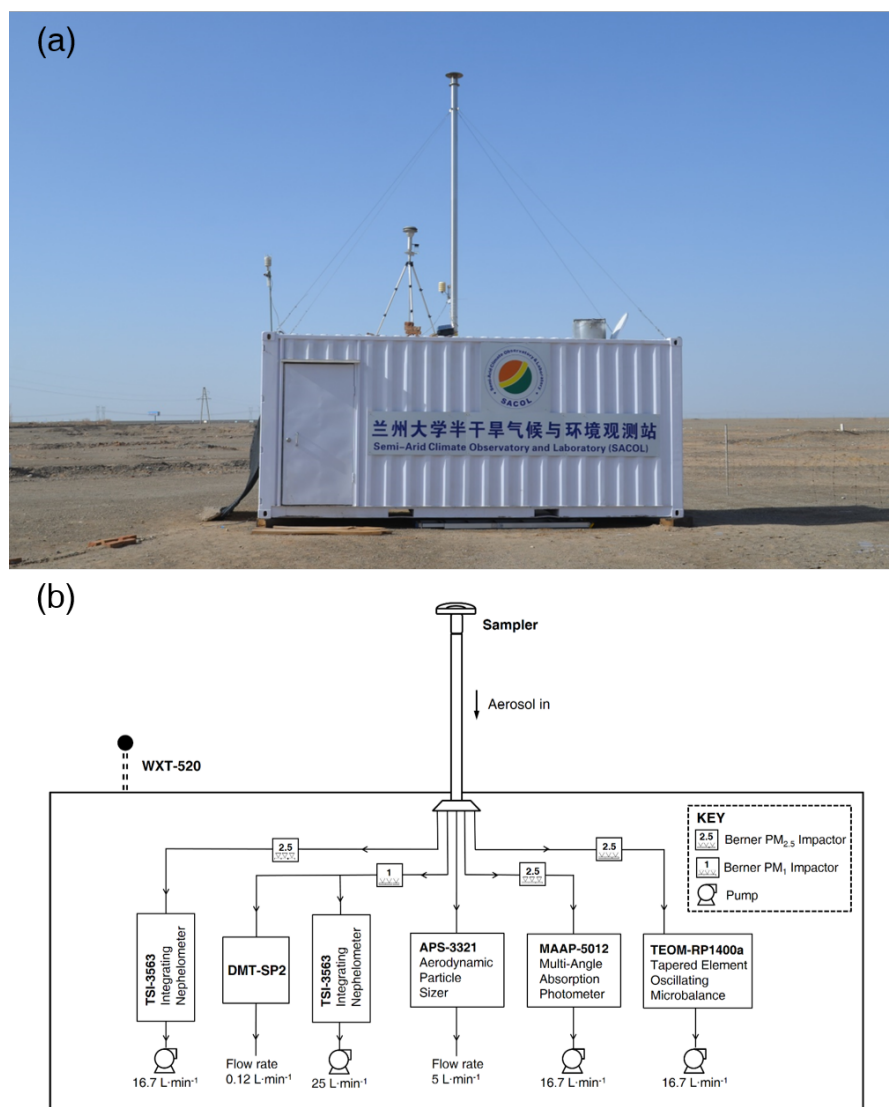
Figure 3. (a) The ground-based mobile laboratory in Dunhuang and **(b)** the schematic diagram of the ensemble instrumentation system.
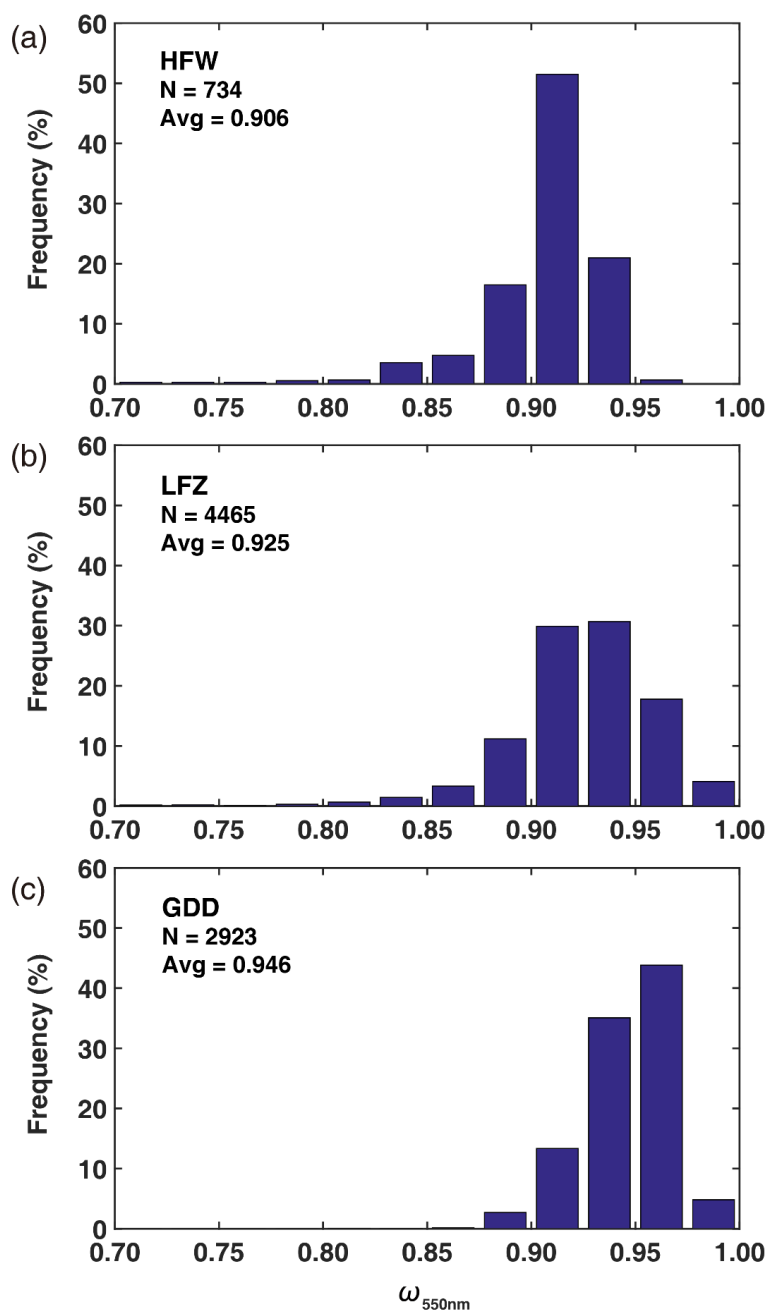
Atmospheric
Chemistry
and Physics
Discussions
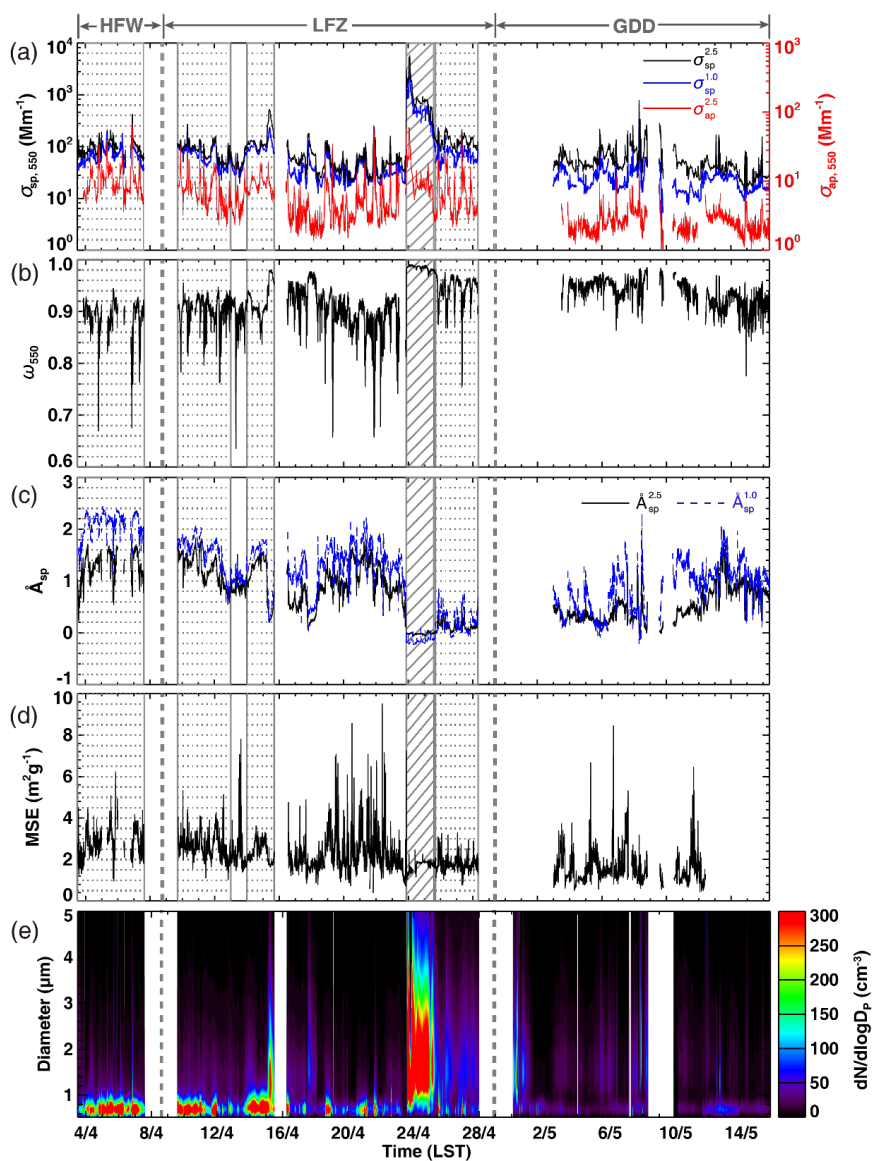
Figure 4. Temporal variations in **(a)** aerosol scattering (absorption) coefficient at 550 nm, **(b)** single scattering albedo at 550 nm, **(c)** scattering Ångström exponent (calculated from 450 nm to 700 nm), **(d)** mass scattering efficiency (MSE) at 550 nm, and **(e)** aerosol size distribution (dN/dlogD$_p$, 0.5 μm< D$_p$<5 μm) during the entire period from 3 April to 16 May 2014. The shaded box represents a strong dust storm that occurred in Zhangye, and the dotted boxes represent four floating dust episodes that occurred in Wuwei and Zhangye.

Atmospheric
Chemistry
and Physics
Discussions
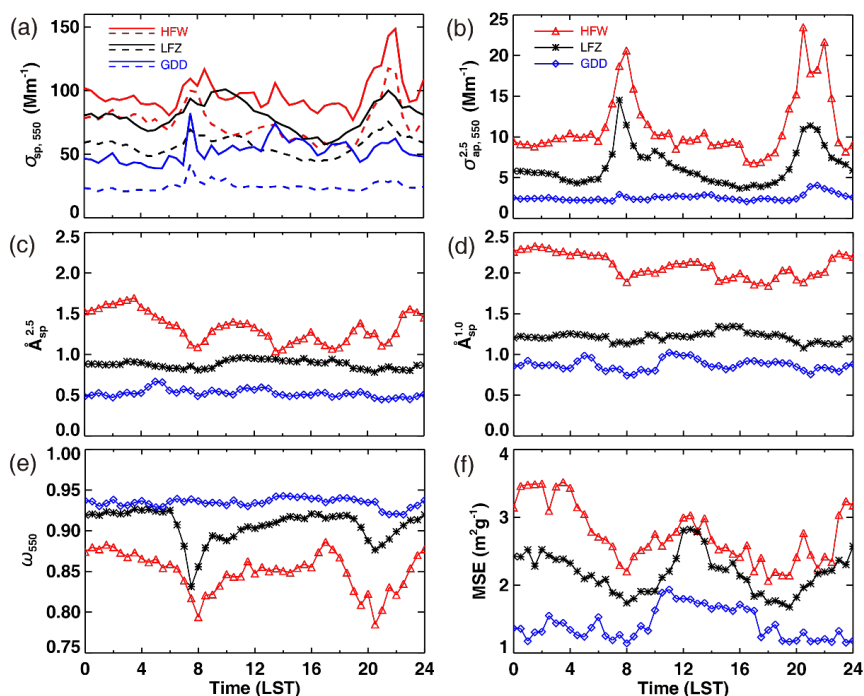
Figure 5. Diurnal variations in **(a)** aerosol scattering coefficient at 550 nm, where solid lines represent the variations in $PM_{2.5}$ and dotted lines represent the variations in $PM_{1.0}$; **(b)** the aerosol absorption coefficient and the scattering Ångström exponent for **(c)** $PM_{2.5}$ and **(d)** $PM_{1.0}$ (both calculated from 450 nm to 700 nm); **(e)** single scattering albedo at 550 nm; and **(f)** mass scattering efficiency (MSE) at 550 nm in Wuwei, Zhangye, and Dunhuang from 3 April to 16 May 2014.
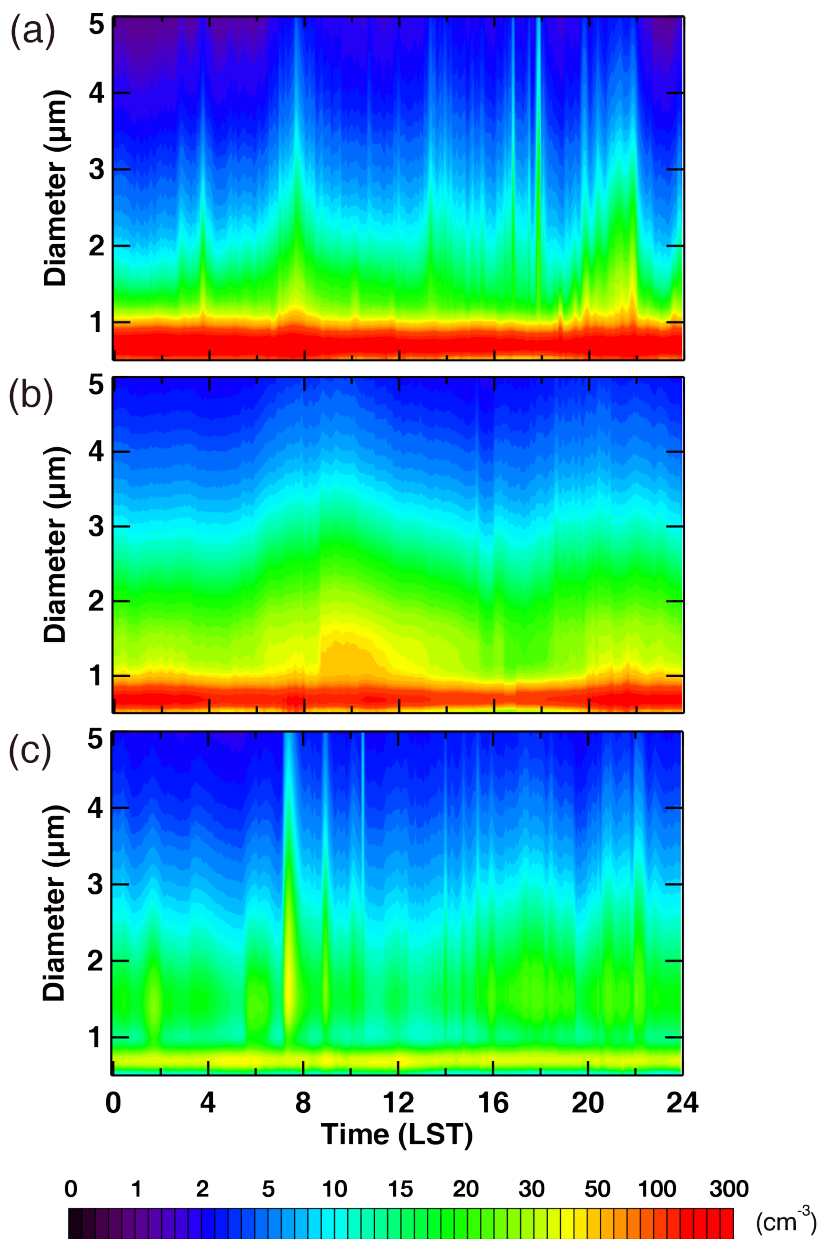
Figure 6. Same as **Figure 5** but for aerosol size distribution (dN/dlogD$_p$, 0.5 μm< D$_p$<5 μm) in **(a)** Wuwei, **(b)** Zhangye, and **(c)** Dunhuang from 3 April to 16 May 2014.

Atmospheric
Chemistry
and Physics
Discussions

Open Access

EGU

Figure 7. Histograms of single scattering albedo at 550 nm in **(a)** Wuwei, **(b)** Zhangye, and **(c)** Dunhuang. The numbers of samples and average values are also shown.

Atmospheric
Chemistry
and Physics
Discussions
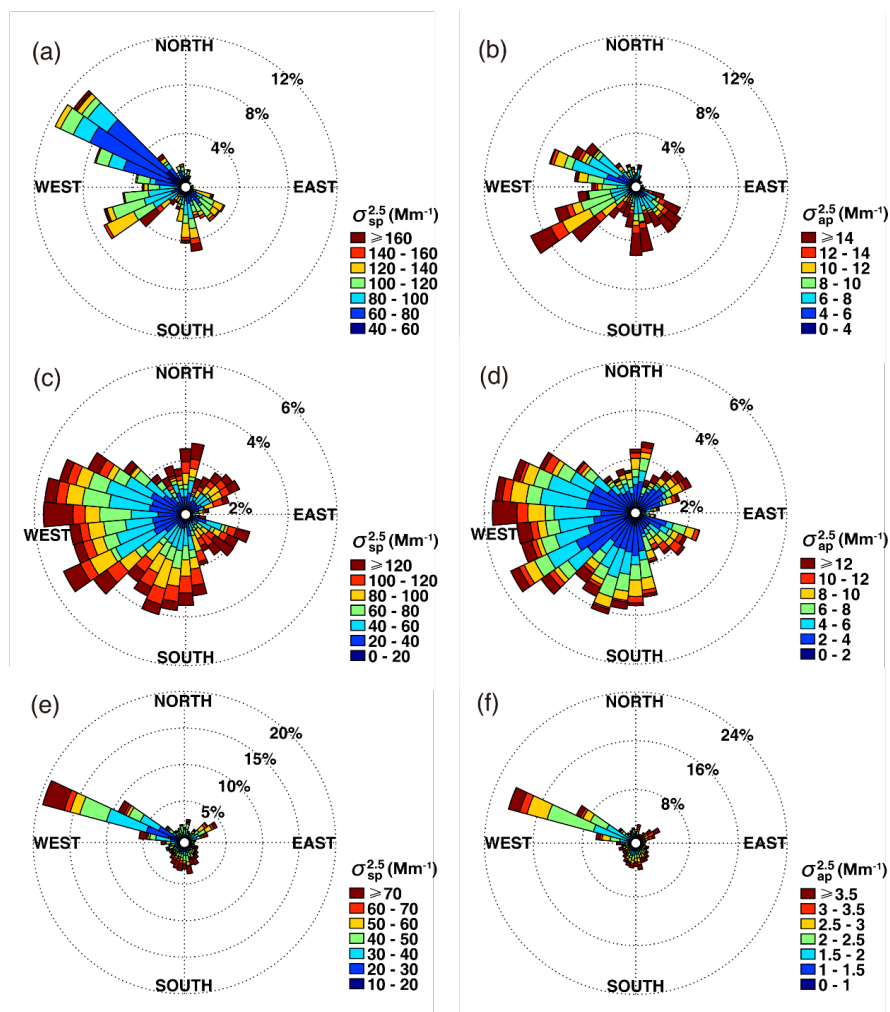
Figure 8. Wind roses for **(a)** aerosol scattering coefficient and **(b)** aerosol absorption coefficient at 550 nm in Wuwei; **(c)** and **(d)** are the same as **(a)** and **(b)** but for Zhangye; and **(e)** and **(f)** are the same as **(a)** and **(b)** but for Dunhuang. Note that data collected during the strong dust storm in Zhangye are excluded.

Atmospheric
Chemistry
and Physics
Discussions
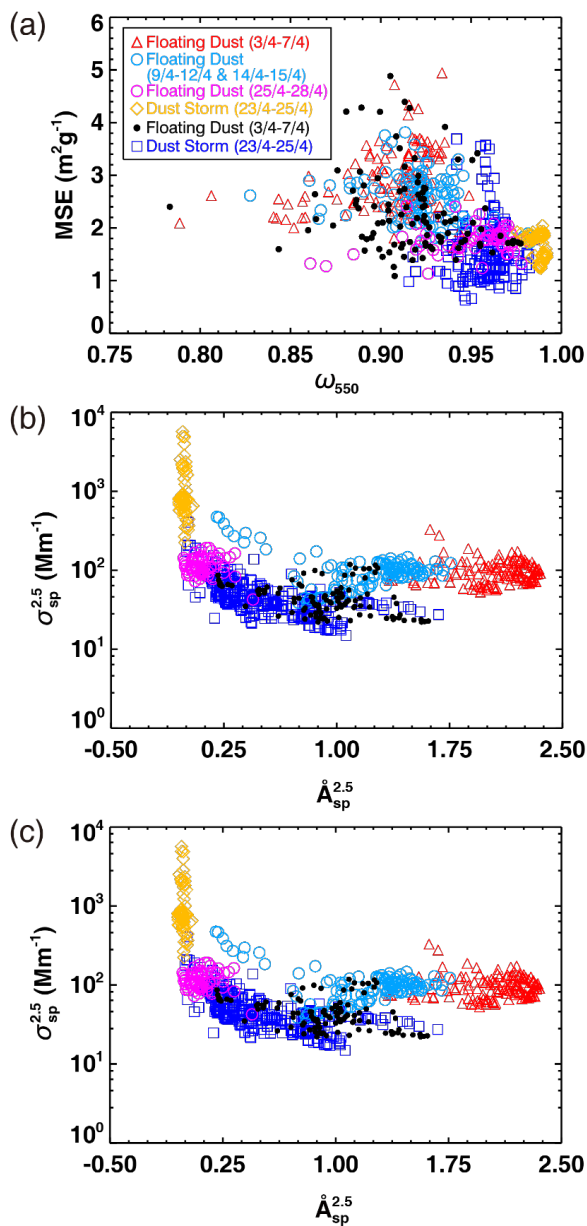
Figure 9. Scatter plots of **(a)** mass scattering efficiency (MSE) versus single scattering albedo (ω) at 550 nm and **(b)** scattering Ångström exponent versus aerosol scattering coefficient for PM$_{2.5}$ at 550 nm; **(c)** is the same as **(b)** but for PM$_{1.0}$.

Atmospheric
Chemistry
and Physics
Discussions
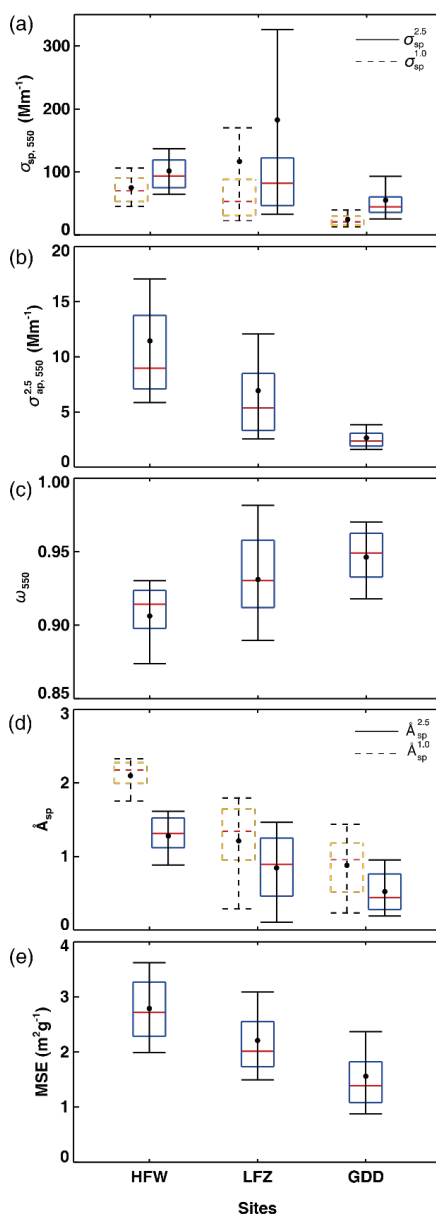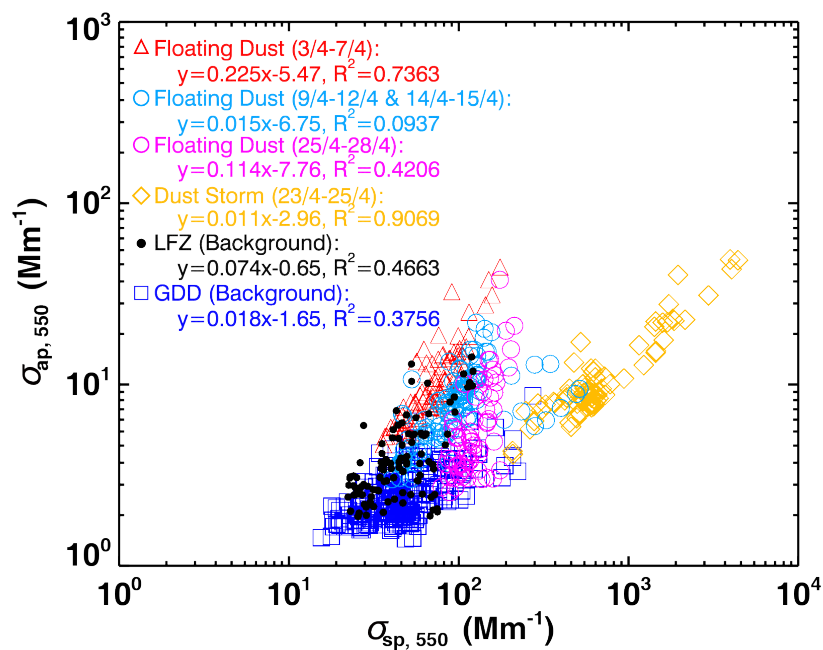

Figure 10. Box plots of (a) scattering coefficient, (b) absorption coefficient, (c) single scattering albedo (ω) at 550 nm, (d) scattering Ångström exponent at 450-700 nm, and (e) mass scattering efficiency (MSE) at 550 nm during the dust field campaign. N represents the number of all in-run datasets in Wuwei (HFW), Zhangye (LFZ), and Dunhuang (GDD). The lines, moving from lower to upper, represent the 10th, 25th, 75th, and 90th percentiles. The red lines and black dots represent the median and mean values, respectively.
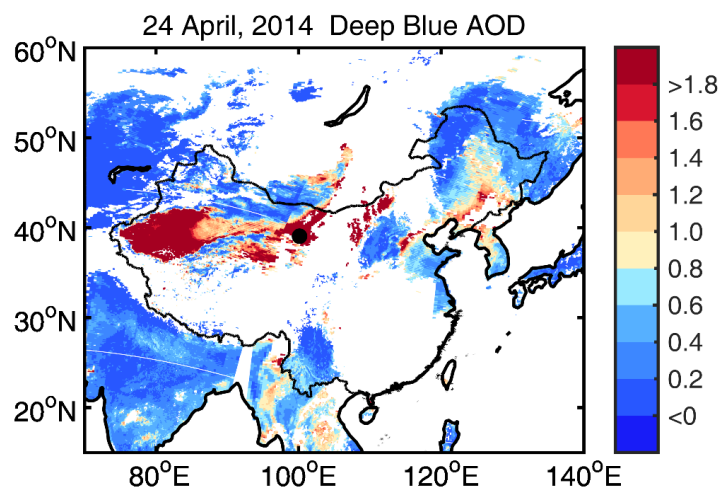
Figure 11. Terra MODIS Deep Blue AOD measured at 550 nm by the NASA Giovanni system during a heavy dust storm on 24 April 2014. The black dot represents the location of the ground-based mobile laboratory at Zhangye.

Figure 12. Scatter plot of aerosol absorption coefficients versus scattering coefficients from 3 April to 16 May 2014. The coloured symbols represent different atmospheric conditions during the dust field campaign.
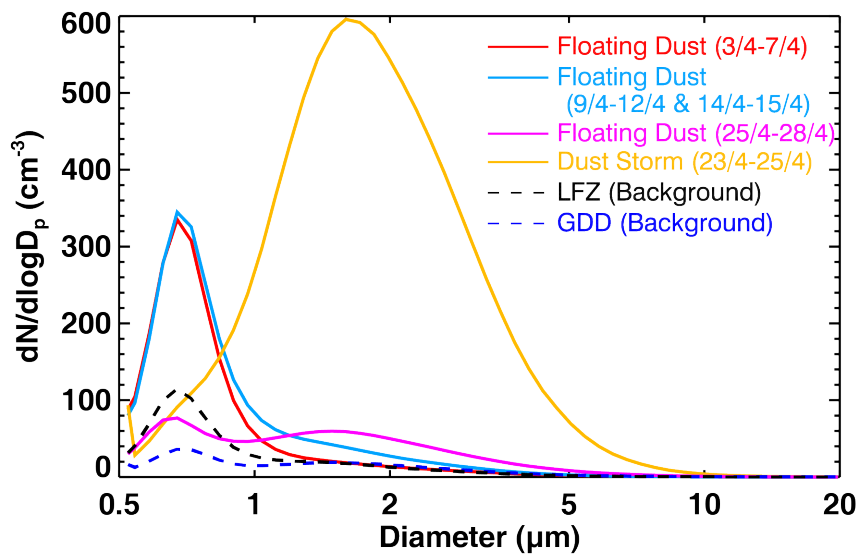
Figure 13. Average aerosol size distribution (dN/dlogD$_p$, cm^{-3}) based on all run data collected during the entire campaign.

Atmospheric
Chemistry
and Physics
Discussions

Table 1. Statistics of optical properties of aerosols measured at three sites.

| | λ (nm) | HFW | LFZ | | | GDD |
			All	No dust	Dust storm	
$\sigma_{sp}^{1.0}$ (Mm^{-1})	450	111.2±41.4	124.6±240.8	70.4±40.4	643.0±548.3	28.7±12.4
	550	74.9±29.1	116.6±260.3	57.1±33.6	686.2±589.7	23.8±11.9
	700	44.0±17.9	104.3±265.4	43.0±27.7	691.4±597.5	20.6±12.2
$\sigma_{sp}^{2.5}$ (Mm^{-1})	450	132.8±49.8	193.4±432.1	98.2±63.2	1088.9±1009.9	58.4±33.0
	550	101.6±39.8	182.6±442.7	84.3±59.1	1108.0±1029.8	53.5±33.4
	700	75.7±32.0	169.2±440.4	70.6±55.3	1097.5±1018.7	48.5±33.0
$\sigma_{ap}^{2.5}$ (Mm^{-1})	550	11.45±7.76	6.93±5.91	6.32±5.01	12.48±9.53	2.65±1.20
ω	550	0.906±0.029	0.931±0.038	0.925±0.035	0.987±0.004	0.946±0.021
Å$_{1.0}$	450–700	2.10±0.24	1.05±0.67	1.18±0.57	-0.15±0.05	0.88±0.44
Å$_{2.5}$	450–700	1.28±0.29	0.77±0.52	0.86±0.48	-0.02±0.02	0.53±0.32
MSE (m^2 g^{-1})	550	2.79±0.68	2.21±0.78	2.26±0.79	1.72±0.23	1.55±0.73

References

Adler, G., Riziq, A. A., Erlick, C., and Rudich, Y.: Effect of intrinsic organic carbon on the optical properties of fresh diesel soot, P. Natl. Acad. Sci. USA, 107, 6699–6704, doi:10.1073/pnas.0903311106, 2010.

Aleksandropoulou, V., Torseth, K., and Lazaridis, M.: Atmospheric Emission Inventory for Natural and Anthropogenic Sources and Spatial Emission Mapping for the Greater Athens Area, Water Air Soil Pollut., 219, 507–526, doi:10.1007/s11270-010-0724-2, 2011.

Anderson, T. L., Covert, D. S., Marshall, S. F., Laucks, M. L., Charlson, R. J., Waggoner, A. P., Ogren, J. A., Caldow, R., Holm, R. L., Quant, F. R., Sem, G. J., Wiedensohler, A., Ahlquist, N. A., and Bates, T. S.: Performance characteristics of a high-sensitivity, three-wavelength total scatter-backscatter nephelometer, J. Atmos. Ocean. Tech., 13, 967–986, 1996.

Arimoto, R., Kim, Y. J., Kim, Y. P., Quinn, P. K., Bates, T. S., Anderson, T. L., Gong, S., Uno, I., Chin, M., Huebert, B. J., Clarke, A. D., Shinozuka, Y., Weber, R. J., Anderson, J. R., Guazzotti, S. A., Sullivan, R. C., Sodeman, D. A., Prather, K. A., and Sokolik, I. N.: Characterization of Asian Dust during ACE-Asia, Global Planet. Change, 52, 23–56, doi:10.1016/j.gloplacha.2006.02.013, 2006.

Bond, T. C. and Bergstrom, R. W.: Light Absorption by Carbonaceous Particles: An Investigative Review, Aerosol Sci. Tech., 40, 27–67, doi:10.1080/02786820500421521, 2006.

Cattrall, C., Carder, K. L., and Gordon, H. R.: Columnar aerosol single-scattering albedo and phase function retrieved from sky radiance over the ocean: measurements of Saharan dust, J. Geophys. Res.-Atmos., 108, 4287, doi:10.1029/2002jd002497, 2003.

Che, H. Z., Wang, Y. Q., and Sun, J. Y.: Aerosol optical properties at Mt. Waliguan Observatory, China, Atmos. Environ., 45, 6004–6009, doi:10.1016/j.atmosenv.2011.07.050, 2011.

Che, H. Z., Wang, Y. Q., Sun, J. Y., Zhang, X. C., Zhang, X. Y., and Guo, J. P.: Variation of Aerosol Optical Properties over the Taklimakan Desert in China, Aerosol Air Qual. Res., 13, 777–785, doi:10.4209/aaqr.2012.07.0200, 2013.

Chen, S. Y., Huang, J. P., Zhao, C., Qian, Y., Leung, L. R., and Yang, B.: Modeling the transport and radiative forcing of Taklimakan dust over the Tibetan Plateau: A case study in the summer of 2006, J. Geophys. Res.-Atmos., 118, 797–812, doi:10.1002/jgrd.50122, 2013.

Dubovik, O., Holben, B. N., Eck, T. F., Smirnov, A., Kaufman, Y. J., King, M. D., Tanré, D., and Slutsker, I.: Variability of absorption and optical properties of key aerosol types observed in worldwide locations, J. Atmos. Sci., 59, 590–608, 2002.

Favez, O., Cachier, H., Sciare, J., Sarda-Esteve, R., and Martinon, L.: Evidence for a significant contribution of wood burning aerosols to PM2.5 during the winter season in Paris, France, Atmos. Environ., 43, 3640–3644, doi:10.1016/j.atmosenv.2009.04.035, 2009.

Ge, J. M., Huang, J. P., Xu, C. P., Qi, Y. L., and Liu, H. Y.: Characteristics of

Atmospheric
Chemistry
and Physics
Discussions

Open Access

EGU

Taklimakan dust emission and distribution: A satellite and reanalysis field perspective, J. Geophys. Res.-Atmos., 119, 11772–11783, doi:10.1002/2014jd022280, 2014.

Ge, J. M., Su, J., Fu, Q., Ackerman, T. P., and Huang, J. P.: Dust aerosol forward scattering effects on ground-based aerosol optical depth retrievals, J. Quant. Spectrosc. Ra., 112, 310–319, doi:10.1016/j.jqsrt.2010.07.006, 2011.

Ginoux, P., Garbuzov, D., and Hsu, H. C.: Identification of anthropogenic and natural dust sources using Moderate Resolution Imaging Spectroradiometer (MODIS) Deep Blue level 2 data, J. Geophys. Res.-Atmos., 115, D05204, doi:10.1029/2009jd012398, 2010.

Goudie, A. S. and Middleton, N. J.: Saharan dust storms: Nature and consequences, Earth-Sci. Rev., 56, 179–204, doi:10.1016/S0012-8252(01)00067-8, 2001.

Gyawali, M., Arnott, W. P., Lewis, K., and Moosmuller, H.: In situ aerosol optics in Reno, NV, USA during and after the summer 2008 California wildfires and the influence of absorbing and non-absorbing organic coatings on spectral light absorption, Atmos. Chem. Phys., 9, 8007–8015, doi: 10.5194/acp-9-8007-2009, 2009.

Hand, J. L. and Malm, W. C.: Review of aerosol mass scattering efficiencies from ground-based measurements since 1990, J. Geophys. Res.-Atmos., 112, D16203, doi:10.1029/2007jd008484, 2007.

Holben, B. N., Eck, T. F., and Fraser, R. S.: Temporal and Spatial Variability of Aerosol Optical Depth in the Sahel Region in Relation to Vegetation Remote-Sensing, Int. J. Remote Sens., 12, 1147–1163, doi: 10.1080/01431169108929719, 1991.

Holben, B. N., Eck, T., Slutsker, I., Smirnov, A., Sinyuk, A., Schafer, J., Giles, D., and Dubovik, O.: AERONET Version 2.0 quality assurance criteria, in: Remote Sensing of the Atmosphere and Clouds, Proc. of SPIE, Goa, India, 13–17 November, 6408, doi:10.1117/12.706524, 2006.

Holben, B. N., Tanre, D., Smirnov, A., Eck, T. F., Slutsker, I., Abuhassan, N., Newcomb, W. W., Schafer, J. S., Chatenet, B., Lavenu, F., Kaufman, Y. J., Castle, J. V., Setzer, A., Markham, B., Clark, D., Frouin, R., Halthore, R., Karneli, A., O'Neill, N. T., Pietras, C., Pinker, R. T., Voss, K., and Zibordi, G.: An emerging ground-based aerosol climatology: Aerosol optical depth from AERONET, J. Geophys. Res.-Atmos., 106, 12067–12097, doi:10.1029/2001jd900014, 2001.

Huang, J. P., Liu, J. J., Chen, B., and Nasiri, S. L.: Detection of anthropogenic dust using CALIPSO lidar measurements, Atmos. Chem. Phys., 15, 11653–11665, doi:10.5194/acp-15-11653-2015, 2015a.

Huang, J. P., Yu, H. P., Guan, X. D., Wang, G. Y., and Guo, R. X.: Accelerated dryland expansion under climate change. Nat. Clim. Change, 6, 166–172, doi:10.1038/nclimate2837, 2015b.

Huang, J. P., Minnis, P., Chen, B., Huang, Z. W., Liu, Z. Y., Zhao, Q. Y., Yi, Y. H., and Ayers, J. K.: Long-range transport and vertical structure of Asian dust from CALIPSO and surface measurements during PACDEX, J. Geophys. Res.-Atmos., 113, D23212, doi:10.1029/2008jd010620, 2008.

Huang, J. P., Minnis, P., Yan, H., Yi, Y., Chen, B., Zhang, L., and Ayers, J. K.: Dust

aerosol effect on semi-arid climate over Northwest China detected from A-Train satellite measurements, Atmos. Chem. Phys., 10, 6863–6872, doi:10.5194/acp-10-6863-2010, 2010.

Huang, J. P., Wang, T. H., Wang, W. C., Li, Z. Q., and Yan, H. R.: Climate effects of dust aerosols over East Asian arid and semiarid regions, J. Geophys. Res.-Atmos., 119, 11398–11416, doi:10.1002/2014jd021796, 2014.

Intergovernmental Panel on Climate Change (IPCC): Climate Change 2013: The Physical Science Basis, Contribution of Working Group I to the Fifth Assessment Report of the Intergovernmental Panel on Climate Change, edited by Stocker, T. F., D. Qin, G.-K. Plattner, M. Tignor, S. K. Allen, J. Boschung, A. Nauels, Y. Xia, V. Bex and P. M. Midgley. Cambridge University Press, Cambridge, United Kingdom and New York, NY, USA, 2013.

Kamani, H., Ashrafi, S. D., Isazadeh, S., Jaafari, J., Hoseini, M., Mostafapour, F. K., Bazrafshan, E., Nazmara, S., and Mahvi, A. H.: Heavy Metal Contamination in Street Dusts with Various Land Uses in Zahedan, Iran, B. Environ. Contam. Tox., 94, 382–386, doi:10.1007/s00128-014-1453-9, 2015.

Kim, W., Doh, S. J., and Yu, Y.: Anthropogenic contribution of magnetic particulates in urban roadside dust, Atmos. Environ., 43, 3137–3144, doi:10.1016/j.atmosenv.2009.02.056, 2009.

Laing, J. R., Jaffe, D. A., and Hee, J. R.: Physical and optical properties of aged biomass burning aerosol from wildfires in Siberia and the Western USA at the Mt. Bachelor Observatory, Atmos. Chem. Phys., 16, 15185–15197, doi:10.5194/acp-16-15185-2016, 2016.

Li, C., Tsay, S.-C., Fu, J. S., Dickerson, R. R., Ji, Q., Bell, S. W., Gao, Y., Zhang, W., Huang, J., Li, Z., and Chen, H.: Anthropogenic air pollution observed near dust source regions in northwestern China during springtime 2008, J. Geophys. Res.-Atmos., 115, doi:10.1029/2009jd013659, 2010.

Li, G. J., Chen, J., Ji, J. F., Yang, J. D., and Conway, T. M.: Natural and anthropogenic sources of East Asian dust, Geology, 37, 727–730, doi:0.1130/g30031a.1, 2009.

Li, J., Wang, Z. F., Zhuang, G., Luo, G., Sun, Y., and Wang, Q.: Mixing of Asian mineral dust with anthropogenic pollutants over East Asia: a model case study of a super-duststorm in March 2010, Atmos. Chem. Phys., 12, 7591–7607, doi:10.5194/acp-12-7591-2012, 2012.

Li, X. Y., Liu, L. J., Wang, Y. G., Luo, G. P., Chen, X., Yang, X. L., Hall, M. H. P., Guo, R. C., Wang, H. J., Cui, J. H., and He, X. Y.: Heavy metal contamination of urban soil in an old industrial city (Shenyang) in Northeast China, Geoderma, 192, 50–58, doi:10.1016/j.geoderma.2012.08.011, 2013.

Li, Z. Q., Lau, W. K. M., Ramanathan, V., Wu, G., Ding, Y., Manoj, M. G., Liu, J., Qian, Y., Li, J., Zhou, T., Fan, J., Rosenfeld, D., Ming, Y., Wang, Y., Huang, J., Wang, B., Xu, X., Lee, S. S., Cribb, M., Zhang, F., Yang, X., Zhao, C., Takemura, T., Wang, K., Xia, X., Yin, Y., Zhang, H., Guo, J., Zhai, P. M., Sugimoto, N., Babu, S. S., and Brasseur, G. P.: Aerosol and monsoon climate interactions over Asia, Rev. Geophys., 54, 866–929, doi:10.1002/2015rg000500, 2016.

Liu, Y., Sato, Y., Jia, R., Xie, Y., Huang, J., and Nakajima, T.: Modeling study on the

transport of summer dust and anthropogenic aerosols over the Tibetan Plateau, Atmos. Chem. Phys., 15, 12581–12594, doi:10.5194/acp-15-12581-2015, 2015.

Mahowald, N. M. and Luo, C.: A less dusty future?, Geophys. Res. Lett., 30, 1903, doi:1910.1029/2003grl017880, 2003.

Menon, S., Hansen, J., Nazarenko, L., and Luo, Y. F.: Climate effects of black carbon aerosols in China and India, Science, 297, 2250–2253, doi:10.1126/science.1075159, 2002.

Mishchenko, M. I., Lacis, A. A., Carlson, B. E., and Travis, L. D.: Nonsphericity of Dust-Like Tropospheric Aerosols – Implications for Aerosol Remote-Sensing and Climate Modeling, Geophys. Res. Lett., 22, 1077–1080, doi:10.1029/95gl00798, 1995.

Nie, W., Ding, A. J., Wang, T., Kerminen, V. M., George, C., Xue, L. K., Wang, W. X., Zhang, Q. Z., Petaja, T., Qi, X. M., Gao, X. M., Wang, X. F., Yang, X. Q., Fu, C. B., and Kulmala, M.: Polluted dust promotes new particle formation and growth, Sci. Rep., 4, 6634, doi:10.1038/srep06634, 2014.

Park, S. U., and Park, M. S.: Aerosol size distributions observed at Naiman in the Asian dust source region of Inner Mongolia, Atmos. Environ., 82, 17–23, doi:10.1016/j.atmosenv.2013.09.054, 2014.

Prospero, J. M., Ginoux, P., Torres, O., Nicholson, S. E., and Gill, T. E.: Environmental characterization of global sources of atmospheric soil dust identified with the Nimbus 7 Total Ozone Mapping Spectrometer (TOMS) absorbing aerosol product, Rev. Geophys., 40, 1002 , doi:10.1029/2000rg000095, 2002.

Pu, W., Wang, X., Zhang, X. Y., Ren, Y., Shi, J. S., Bi, J. R., and Zhang, B. D.: Size Distribution and Optical Properties of Particulate Matter (PM10) and Black Carbon (BC) during Dust Storms and Local Air Pollution Events across a Loess Plateau Site, Aerosol Air Qual. Res., 15, 2212–2224, doi:10.4209/aaqr.2015.02.0109, 2015.

Qian, W. H., Tang, X., and Quan, L. S.: Regional characteristics of dust storms in China, Atmos. Environ., 38, 4895–4907, doi:10.1016/j.atmosenv.2004.05.038, 2004.

Ramanathan, V., Chung, C., Kim, D., Bettge, T., Buja, L., Kiehl, J. T., Washington, W. M., Fu, Q., Sikka, D. R., and Wild, M.: Atmospheric brown clouds: Impacts on South Asian climate and hydrological cycle, P. Natl. Acad. Sci. USA, 102, 5326–5333, doi:10.1073/pnas.0500656102, 2005.

Ramanathan, V., Crutzen, P. J., Kiehl, J. T., and Rosenfeld, D.: Atmosphere - Aerosols, climate, and the hydrological cycle, Science, 294, 2119–2124, doi:10.1126/science.1064034, 2001.

Ramanathan, V., Ramana, M. V., Roberts, G., Kim, D., Corrigan, C., Chung, C., and Winker, D.: Warming trends in Asia amplified by brown cloud solar absorption, Nature, 448, 575–578, doi:10.1038/nature06019, 2007.

Rosenfeld, D., Clavner, M., and Nirel, R.: Pollution and dust aerosols modulating tropical cyclones intensities, Atmos. Res., 102, 66–76, doi:10.1016/j.atmosres.2011.06.006, 2011.

Rosenfeld, D., Rudich, Y., and Lahav, R.: Desert dust suppressing precipitation: A possible desertification feedback loop, Proc. Natl. Acad. Sci., 98, 5975–5980,

Atmospheric
Chemistry
and Physics
Discussions

doi:10.1073/pnas.101122798, 2001.

Shi J. S., Tian P. F., Zhou T., and Huang Z. W.: Aerosol optical properties in spring in Agricultural area in Hexi Corridor, J. Arid Meteo., 33, 38–44, doi:10.11755/j.issn.1006-7639(2015)-01-0038, 2015 (in Chinese).

Shi J. S., Zhao M. G., Ge J. M., Bi J. R., Wang X., and Chen M.: The calibration of three-wavelength integration nephelometer, China Environ. Sci., 33, 1372–1378, 2013 (in Chinese).

Spracklen, D. V., and Rap, A.: Natural aerosol-climate feedbacks suppressed by anthropogenic aerosol, Geophys. Res. Lett., 40, 5316–5319, doi:10.1002/2013gl057966, 2013.

Srivastava, K. and Bhardwaj, R.: Analysis and very short range forecast of cyclone "AILA" with radar data assimilation with rapid intermittent cycle using ARPS 3DVAR and cloud analysis techniques, Meteorol. Atmos. Phys., 124, 97–111, doi:10.1007/s00703-014-0307-7, 2014.

Tao, J., Zhang, L., Cao, J., and Zhang, R.: A review of current knowledge concerning PM2. 5 chemical composition, aerosol optical properties and their relationships across China, Atmos. Chem. Phys., 17, 9485-9518, https://doi.org/10.5194/acp-17-9485-2017, 2017.

Tao, J., Zhang, L., Gao, J., Wang, H., Chai, F., and Wang, S.: Aerosol chemical composition and light scattering during a winter season in Beijing, Atmos. Environ., 110, 36-44, 2015.

Tao, J., Zhang, L., Ho, K., Zhang, R., Lin, Z., Zhang, Z., Lin, M., Cao, J., Liu, S., and Wang, G.: Impact of PM2.5 chemical compositions on aerosol light scattering in Guangzhou - the largest megacity in South China, Atmos. Res., 135–136, 48–58, 2014.

Tegen, I., and Fung, I.: Contribution to the Atmospheric Mineral Aerosol Load from Land-Surface Modification, J. Geophys. Res.-Atmos., 100, 18707–18726, doi:10.1029/95jd02051, 1995.

Tegen, I., Harrison, S. P., Kohfeld, K. E., Engelstaedter, S., and Werner, M.: Emission of soil dust aerosol: Anthropogenic contribution and future changes, Geochim. Cosmochim. Ac., 66, A766, 2002.

Tegen, I., Werner, M., Harrison, S. P., and Kohfeld, K. E.: Relative importance of climate and land use in determining present and future global soil dust emission. Geophys. Res. Lett., 31, L05105, doi:10.1029/2003gl019216, 2004.

Thompson, L. G., Davis, M. E., Mosleythompson, E., and Liu, K. B.: Pre-Incan Agricultural Activity Recorded in Dust Layers in 2 Tropical Ice Cores, Nature, 336, 763–765, doi:10.1038/336763a0, 1988.

Wang, X., Doherty, S. J., and Huang, J.: Black carbon and other light–absorbing impurities in snow across Northern China, J. Geophys. Res.-Atmos., 118, 1471–1492, doi:10.1029/2012jd018291, 2013.

Wang, X., Huang, J. P., Zhang, R. D., Chen, B., and Bi, J. R.: Surface measurements of aerosol properties over northwest China during ARM China 2008 deployment, J. Geophys. Res.-Atmos., 115, doi:10.1029/2009jd013467, 2010.

Wang, X., Huang, J., Ji, M., and Higuchi, K.: Variability of East Asia dust events and

Atmospheric
Chemistry
and Physics
Discussions

their long-term trend, Atmos. Environ., 42, 3156–3165, doi:10.1016/j.atmosenv.2007.07.046, 2008.

Wang, X., Pu, W., Zhang, X., Ren, Y., and Huang, J.: Water-soluble ions and trace elements in surface snow and their potential source regions across northeastern China, Atmos. Environ., 114, 57–65, doi:10.1016/j.atmosenv.2015.05.012, 2015.

Washington, R., Todd, M., Middleton, N. J., and Goudie, A. S.: Dust-storm source areas determined by the total ozone monitoring spectrometer and surface observations, Ann. Assoc. Am. Geogr., 93, 297–313, doi:10.1111/1467-8306.9302003, 2003.

Xin, J. Y., Du, W. P., Wang, Y. S., Gao, Q. X., Li, Z. Q., and Wang, M. X.: Aerosol Optical Properties Affected by a Strong Dust Storm over Central and Northern China, Adv. Atmos. Sci., 27, 562–574, doi:10.1007/s00376-009-9023-5, 2010.

Xin, J. Y., Wang, S. G., Wang, Y. S., Yuan, J. Y., Zhang, W. Y., and Sun, Y.: Optical properties and size distribution of dust aerosols over the Tengger Desert in Northern China, Atmos. Environ., 39, 5971–5978, doi:10.1016/j.atmonsenv.2005.06.027, 2005.

Xin, J. Y., Wang, Y. S., Pan, Y. P., Ji, D. S., Liu, Z. R., Wen, T. X., Wang, Y. H., Li, X. R., Sun, Y., Sun, J., Wang, P. C., Wang, G. H., Wang, X. M., Cong, Z. Y., Song, T., Hu, B., Wang, L. L., Tang, G. Q., Gao, W. K., Guo, Y. H., Miao, H. Y., Tian, S. L., and Wang, L.: The Campaign on Atmospheric Aerosol Research Network of China Care-China, B. Am. Meteorol. Soc., 96, 1137–1155, doi:10.1175/BAMS-D-14-00039.1, 2015.

Yang, M., Howell, S. G., Zhuang, J., and Huebert, B. J.: Attribution of aerosol light absorption to black carbon, brown carbon, and dust in China – interpretations of atmospheric measurements during EAST-AIRE, Atmos. Chem. Phys., 9, 2035–2050, doi:10.5194/acp-9-2035-2009, 2009.

Zhang, R., Hegg, D. A., Huang, J., and Fu, Q.: Source attribution of insoluble light-absorbing particles in seasonal snow across northern China, Atmos. Chem. Phys., 13, 6091–6099, doi:10.5194/acp-13-6091-2013, 2013.

Zhang, X. Y., Arimoto, R., and An, Z. S.: Dust emission from Chinese desert sources linked to variations in atmospheric circulation, J. Geophys. Res.-Atmos., 102, 28041–28047, doi:10.1029/97jd02300, 1997.

Zhang, X. Y., Wang, L., Wang, W. H., Cao, D. J., Wang, X., and Ye, D. X.: Long-term trend and spatiotemporal variations of haze over China by satellite observations from 1979 to 2013, Atmos. Environ., 119, 362–373, doi:10.1016/j.atmosenv.2015.08.053, 2015.

Zhang, X. Y., Wang, Y. Q., Wang, D., Gong, S. L., Arimoto, R., Mao, L. J., and Li, J.: Characterization and sources of regional-scale transported carbonaceous and dust aerosols from different pathways in coastal and sandy land areas of China, J. Geophys. Res.-Atmos., 110, D15301, doi:10.1029/2004jd005457, 2005.